




## RESEARCH ARTICLE

# Tuning the demodulation frequency based on a normalized trajectory model for mobile underwater acoustic communications

Abdel-Mehsen Ahmad<sup>1,2</sup> | Michel Barbeau<sup>3</sup>  | Joaquin Garcia-Alfaro<sup>4</sup>  |  
Jamil Kassem<sup>1,4</sup> | Evangelos Kranakis<sup>3</sup> 

<sup>1</sup>School of Engineering, Lebanese International University, Bekaa, Lebanon

<sup>2</sup>School of Engineering, International University of Beirut, Beirut, Lebanon

<sup>3</sup>School of Computer Science, Carleton University, Ottawa, Ontario, Canada

<sup>4</sup>Institut Polytechnique de Paris, Telecom SudParis, CNRS Samovar UMR 5157, Institut Mines-Telecom, Evry, France

## Correspondence

Joaquin Garcia-Alfaro, Institut Polytechnique de Paris, Telecom SudParis, CNRS Samovar UMR 5157, Institut Mines-Telecom, 9 Rue Charles Fourier, 91000 Evry, France.  
Email: jgalfaro@ieee.org

## Abstract

We have developed a demodulator for low data rate, asynchronous frame, and narrow bandwidth underwater acoustic communication. We aim at operation under harsh conditions, ie, low signal-to-noise ratio, and across long distances. In this paper, we pay a special attention to the efficiency of mobility support. Mobility results into the Doppler effect, which, for a demodulator, makes the carrier frequency drift arbitrarily during attempts to decode frames. The chances of success are better when the demodulator can tune into the drifted carrier frequency. This can be achieved by trying a range of possible drifted carriers. We introduce the novel idea of normalized trajectory. Each normalized trajectory produces a unique Doppler shift pattern that can be applied to tune into a drifted carrier. We demonstrate that this improvement is theoretically sound. From a practical point of view, the search space is potentially reduced. The actual gain in performance is application-specific and depends on the actual sets of trajectory parameters that are considered. We introduce the concept of normalized trajectory, discuss its integration into the demodulator, and review the performance of the new design.

## 1 | INTRODUCTION

Underwater acoustic data communication finds applications in monitoring and surveillance of coastal waters,<sup>1</sup> submarine activity sensors,<sup>2</sup> autonomous undersea vehicles,<sup>3</sup> and submerged airplane locator beacons. Our focus is on low-frequency mobile underwater communications,<sup>4,5</sup> ie, in the range 0.3 to 3 kHz. This acoustic band is interesting because, relative to other bands, the attenuation is lower, a fact already highlighted by Stojanovic.<sup>6</sup> Indeed, the potential for long distance contacts has been demonstrated.<sup>7</sup> Nevertheless, due to the limited half-power bandwidth of low-frequency and long-distance operation, only extremely low data rates can be reasonably envisioned.

In this paper, we pay special attention to mobility support. The relative mobility of a transmitter w.r.t. a receiver affects the acoustic underwater communication frequency. This is called the Doppler effect. In a previous work, we have identified various patterns of frequency drift due to the Doppler effect.<sup>8,9</sup> There are three main cases: constant, linearly variable, and nonlinearly variable Doppler shift. The latter is the most challenging one to handle. We have developed a pragmatic solution.<sup>10</sup> We assume that vehicles are traveling according to straight-line trajectories. We believe the assumption is realistic and practical for the maritime environment because vessels tend to follow routes that comprise long straight-line segments. We model plausible straight-line trajectories and calculate the corresponding Doppler shifted carriers. During demodulation, the receiver tunes into these drifted carriers and search for data signals. This strategy produces good

performance results, as reported in the work of Ahmad et al.<sup>10</sup> In this paper, we introduce an improvement. In our initial modem design, several redundant cases are generated and examined. An example is presented in Figure 1. On this nautical chart, there is a receiver at location  $q$  and two mobile transmitters at locations  $p_1$  and  $p_2$ . The motions of the mobiles are specified by velocity vectors  $\vec{V}_1$  and  $\vec{V}_2$ . The vectors have the same magnitude. Their lines of action are represented by the dotted lines. Because the transmitters are in motion, the frequency of their signal is changed. In this example, they are both moving away from the receiver. Hence, their signal is subject to a negative drift, which varies in time in a non-linear way. Figure 2 plots the frequency drift (Hz) as a function of time (second). For a period of 110 seconds, at 1.5 kHz and 10 m/s, the drift goes from slightly above  $-1.2$  Hz to slightly below  $-2.2$  Hz. The important remark to make is that relative to the position of the receiver, both trajectories produce the same Doppler effect pattern, pictured in Figure 2. The Doppler effects are the same due to the symmetries in the trajectories in Figure 1. Relative to the position of the receiver  $q$ , both mobiles produce the same frequency drift patterns. A well-crafted normalization mapping would identify such symmetries and equivalent trajectories, with respect to the Doppler effect at a receiver. This is exactly the aim of this paper. For the example of Figure 2, in both cases, the relative velocity is the same, Doppler effect-wise. They can be treated as the same case.

Acknowledging that the Doppler effect is a relative phenomenon between a transmitter and a receiver, we introduce in this paper the novel concept of normalized trajectory. A normalized trajectory generates a unique Doppler shift pattern and corresponding shifted carrier. In a new design, the demodulator tunes solely into carriers generated from normalized trajectories. Each such drifted carrier is unique. Because redundancy is eliminated, the cost of demodulation is reduced when the search for signals with nonlinear drifted carriers is performed. The actual gain in performance is application-specific and depends on the actual sets of trajectory parameters that are considered. Resource requirements are lower and the demodulator can be implemented on smaller platforms.

This article builds upon a Doppler shift analysis<sup>8,9</sup> and a modem design for communication with slow-rate data frames carried by low-frequency underwater acoustic signals.<sup>11</sup> It extends our previous work on Doppler effect handling<sup>10</sup> with the concept of normalized trajectory model. Our contribution is about Doppler compensation. This particular topic has been studied before in the context of underwater communication<sup>12-15</sup> and for classical wireless communication.<sup>16</sup> All previous studies proposed solutions for constant Doppler shifts (during the reception of a frame). In our work, we assume and propose a solution for variable Doppler shifts, linear and nonlinear. This practical problem is very challenging. It

**FIGURE 1** Nautical map picturing two different straight-line trajectories

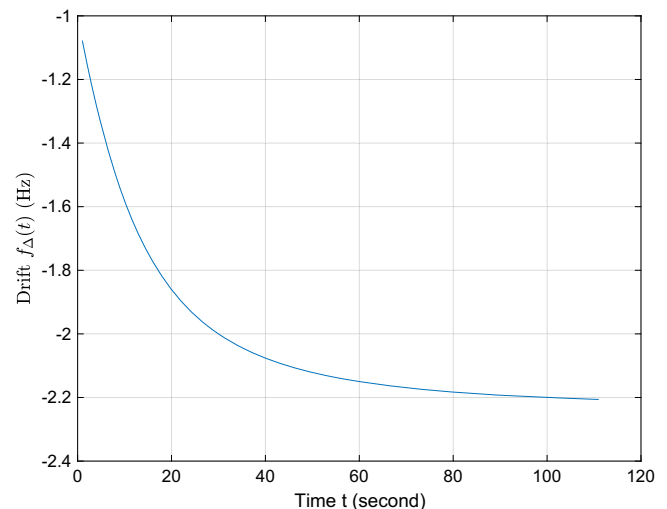
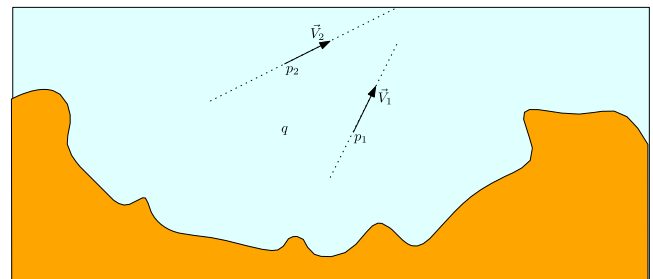


**FIGURE 2** Equivalent Doppler effect due to symmetry

is highly relevant for mobile slow-speed underwater communications, which are useful for very noisy conditions such as those present in the long-range underwater environment. To the best of our knowledge, this problem has received very little attention. In our paper, we propose a method for efficiently (time complexity is cubic) compensating variable nonlinear Doppler effects.

Related work is reviewed in more detail in Section 2. The idea of normalized trajectory model that yields unique Doppler shift patterns is presented in Section 3. The integration of the normalized trajectory model into the demodulator is detailed in Section 4. Performance is discussed in Section 5. We conclude with Section 6.

## 2 | RELATED WORK

This paper is about sending and receiving data packets under the sea surface between mobile vehicles. Techniques for underwater communication include cables, electromagnetic waves, optical waves, and acoustics waves. Cables are impractical for mobile communication but useful for underwater robotics.<sup>17</sup> The conductivity nature of electromagnetic waves in the underwater environment makes them usable only for distances limited to a few meters<sup>18,19</sup> and requires powerful transmitters.<sup>20</sup> Underwater optical waves are quickly absorbed and limited to short ranges.<sup>20</sup> In contrast, acoustic waves are subject to relatively lower absorption, in particular at low frequencies, and enable long-range communications, in the order of kilometers.<sup>6</sup> However, acoustic waves also have their challenges such as low propagation speed, reverberation due to multipath propagation, and relatively narrow bandwidth, which means low data rates.<sup>21</sup>

Underwater acoustic modems are used to establish under sea communication links. Commercial modems are available, but their proprietary nature makes their use difficult for experimenting new physical and link layer communication strategies. The software-defined radio (SDR)<sup>22,23</sup> approach is ideal for experimentation and research on communication, in particular with open platforms such as GNU Radio.<sup>24</sup> It is a platform where components of a modem architecture such as filters and decoders are implemented in software. For underwater applications, the SDR is interfaced with the analog world using a hydrophone, in reception, and a vibrator, in transmission.

The SDR approach has been adopted by a number of underwater acoustic modem projects. Dol et al authored a survey of projects.<sup>25</sup> For example, the modem of Borowski and Duchamp<sup>26</sup> does four-tone frequency-shift keying (4-FSK) and frequency division multiplexing (FDM). A receiver has the capability to send feedback to a transmitter w.r.t. the channel impulse response used for equalization. Demirors et al.<sup>27</sup> proposed a modem based on orthogonal frequency-division multiplexing (OFDM) and direct sequence spread spectrum (DSSS). A transmitter adapts to the channel conditions based on feedback returned by a sender. There is an acknowledgement-based link layer with IPv4 and IPv6 support at the network layer. As alternatives to the SDR approach, Cario et al<sup>28</sup> have implemented their modem on a DSP board, whereas Benson et al<sup>29</sup> did it on field-programmable gate array. More recent results on underwater modem design include the work of Goncalves et al<sup>30</sup> on OFDM and Demirors et al<sup>31</sup> on high-speed communications.

An issue related to mobility is the Doppler effect. This issue has received some attention. The 4-FSK-DSSS modem of Wu et al<sup>14</sup> estimates how a carrier is affected by the Doppler shift. The receiver compares the time required to send a packet and the time to receive it. The ratio of the former over the latter is proportional to the frequency drift due the Doppler effect and used to tune the carrier frequency. For their OFDM modem, Huang and Lawrence use a pilot signal.<sup>32</sup> Chen et al also computes a scaling factor using pilot signals.<sup>33</sup> These approaches can compensate a constant Doppler shift (see Case 1 in Section 4). Other approaches for constant Doppler shift compensation (not all necessarily in the context of underwater communications) have been proposed by Sharif et al,<sup>12</sup> Li et al,<sup>13</sup> Kim et al,<sup>16</sup> Ming et al,<sup>15</sup> Huang et al,<sup>34</sup> Amar et al,<sup>35</sup> Jing et al,<sup>36</sup> Li et al,<sup>37</sup> Lu et al,<sup>38</sup> Zhang et al,<sup>39</sup> Yu et al,<sup>40</sup> Hou et al,<sup>41</sup> and Huang et al.<sup>42</sup> In our modem design (Sections 3 and 4), we address variable Doppler shifts, which can be linear and nonlinear. We have addressed the linear case in a previous work.<sup>11</sup> The contribution presented in this paper specifically addresses the nonlinear case. At a low underwater data rate, this issue is highly relevant because frames are long lasting (111 seconds in our design). Our previous analysis<sup>9</sup> has shown that the Doppler shift can vary significantly during the transmission of a frame. In this context, the compensation of variable Doppler shift needs special attention and can increase performance.<sup>10</sup> Our Doppler compensation approach is based on a trajectory model presented in detail in Section 3. Underwater mobility modeling has been addressed before but mainly to study connectivity in sensor networks.<sup>43,44</sup>

Mobile underwater communication is used for industrial, scientific, and defense applications.<sup>45</sup> Applications include environmental monitoring, observing ocean floor geological processes, monitoring water characteristics, marine life

pollution, climate changes, and global warming. Industrial applications encompass oil and mineral extraction, underwater pipelines, and commercial fisheries. Underwater sensor networks are also envisioned for defense applications such as the monitoring of port facilities and surveillance of coastal waters.

Jones et al<sup>46</sup> discuss the use of an autonomous underwater glider for Arctic-like conditions with several months of autonomy. For the same conditions, Freitag et al<sup>7</sup> developed a system for long-range navigation and acoustic communication for underwater unmanned vehicles. Dong et al<sup>47</sup> proposed a modem autonomous underwater vehicles. Special attention is given to energy efficiency.

An issue that is occasionally raised is the environmental impact of underwater communication, in particular on marine life. A recent study by Bernaldo de Quiros et al<sup>48</sup> discusses the impact that antisubmarine sonars have on beaked whales (in particular for midfrequency sonars in the 3 to 4 kHz range). To the best of our knowledge, there is no similar study specifically for underwater communication. However, some modem designs give a particular importance to environmental impact. For example, Li et al<sup>49</sup> designed an underwater acoustic modem that avoids interference with dolphin signals.

### 3 | NORMALIZED TRAJECTORY MODEL

The demodulation of signals subject to nonlinear Doppler effects is a problem for long-lasting data frames (111 seconds/frame in our modem design). Tracking the carrier frequency along the symbols of a frame increases the chances of successful demodulation. Due to the Doppler effect, the carrier frequency may drift according to several different and erratic patterns. We approach the problem pragmatically, making assumptions about the cause of the Doppler effect. In the underwater environment, assumptions can be made about positions, trajectories, and velocities. It is reasonable to assume location and velocity awareness.<sup>50</sup> It is also plausible to suppose that a peer is traveling along a sea route or a navigation channel. Assumptions can also be made regarding velocities.<sup>3</sup> We assume straight-line trajectory models for mobile communicating vehicles and infer the corresponding Doppler effect on the frequency. During the search for signals in a spectrum of frequency, we try a number of patterns of drifted carrier frequencies determined by plausible vehicle starting positions and parameters of their straight-line trajectories. We assume that this information will be provided by a person knowledgeable of the environment in which the modem is going to operate. The knowledgeable person needs to provide information about plausible starting positions, sea routes, navigation channels, and velocities of underwater vehicles. This information is used to determine the parameters of plausible trajectory models. The latter are used to infer plausible Doppler shift patterns. Exploration of these Doppler shift patterns enables successful demodulation of frames that would not be received with success otherwise.

In this section, we first develop a straight-line trajectory model. A trajectory normalizer is introduced. It maps each of the trajectories to a unique trajectory model, together with the corresponding Doppler effect.

#### 3.1 | Straight-line trajectories

We model the Doppler effect between two communicating mobile vehicles. We assume that the vehicles are following straight-line trajectories and moving at constant velocities. We define the concept of straight-line trajectory in the Cartesian representation. We translate the Cartesian representation to the parametric form. The Doppler effect is calculated in the parametric form. For the sake of simplicity, we develop the equations for the two-dimensional Euclidean plane. Similar equations can be elaborated for the three-dimensional Euclidean space.

Two vehicles  $R_a$  and  $R_b$  are moving along straight lines specified by the standard Cartesian equations

$$y = m_a x + c_a \text{ and } y = m_b x + c_b. \quad (1)$$

The parameters  $m_a$  and  $m_b$  are the slopes of the lines. The parameters  $c_a$  and  $c_b$  are constants. In the parametric form, the initial positions of the vehicles are defined by the coordinates  $a = (a_1, a_2)$  and  $b = (b_1, b_2)$ . We have the following two equivalences:

$$a_2 = m_a a_1 + c_a \text{ and } b_2 = m_b b_1 + c_b. \quad (2)$$

The vehicles are moving at constant velocities  $v_a$  and  $v_b$ . On their respective straight-line trajectories, let  $P_a(t)$  and  $P_b(t)$  be the positions of the vehicles at time  $t$ . From their starting positions, let  $x_a(t), y_a(t)$  and  $x_b(t), y_b(t)$  be the horizontal

and vertical distances traversed by the vehicles at time  $t$ . Given that the vehicles are moving at constant velocities, their positions satisfy the following conditions:

$$P_a(t) = [a_1 + x_a(t), a_2 + y_a(t)] \text{ and } P_b(t) = [b_1 + x_b(t), b_2 + y_b(t)]. \quad (3)$$

Note that  $x_a(0), y_a(0), x_b(0)$ , and  $y_b(0)$  are all null. Because the vehicles are moving on straight lines, we have, by definition, that

$$y_a(t) = m_a x_a(t) \text{ and } y_b(t) = m_b x_b(t). \quad (4)$$

Moreover, due to their constant velocities, we have that

$$x_a^2(t) + y_a^2(t) = (v_a t)^2 \text{ and } x_b^2(t) + y_b^2(t) = (v_b t)^2. \quad (5)$$

Combining Equations (4) and (5), we conclude that the corresponding horizontal and vertical offsets for vehicle  $R_a$  are  $x_a(t) = v_a t / \sqrt{1 + m_a^2}$  and  $y_a(t) = m_a v_a t / \sqrt{1 + m_a^2}$ . Similar equations can be developed for vehicle  $R_b$ . As a function of time  $t$ , the positions of the vehicles are given by the equations

$$P_a(t) = \vec{A}t + a \text{ and } P_b(t) = \vec{B}t + b, \quad (6)$$

with velocity vectors defined as

$$\vec{A} = \left( \frac{v_a}{\sqrt{1 + m_a^2}}, \frac{m_a v_a}{\sqrt{1 + m_a^2}} \right) \text{ and } \vec{B} = \left( \frac{v_b}{\sqrt{1 + m_b^2}}, \frac{m_b v_b}{\sqrt{1 + m_b^2}} \right). \quad (7)$$

Let  $\vec{P}_b(t)$  and  $\vec{P}_a(t)$  be the vectors starting at the origin and ending at points  $P_b(t)$  and  $P_a(t)$ . Let  $\vec{P}'_a(t)$  and  $\vec{P}'_b(t)$  be the first derivatives of vectors  $\vec{P}_b(t)$  and  $\vec{P}_a(t)$ . As depicted in Figure 3, vector  $\vec{U}(t)$  is equal to the difference  $\vec{P}_b(t) - \vec{P}_a(t)$ . We project vectors  $\vec{P}'_a(t)$  and  $\vec{P}'_b(t)$  onto the vector  $\vec{U}(t)$ , forming the corresponding projection vectors  $\vec{Pr}j_a(t)$  and  $\vec{Pr}j_b(t)$ . The equation of the vector  $\vec{Pr}j_a(t)$ , that is, the projection of vector  $\vec{P}'_a(t)$  on the vector  $\vec{U}(t)$ , is

$$\vec{Pr}j_a(t) = \|\vec{P}'_a(t)\| \cdot \frac{\langle \vec{P}'_a(t), \vec{U}(t) \rangle}{\|\vec{P}'_a(t)\| \cdot \|\vec{U}(t)\|} \cdot \frac{\vec{U}(t)}{\|\vec{U}(t)\|} = \frac{\langle \vec{P}'_a(t), \vec{U}(t) \rangle}{\|\vec{U}(t)\|} \cdot \frac{\vec{U}(t)}{\|\vec{U}(t)\|},$$

where  $\langle \cdot, \cdot \rangle$  denotes the inner product of two vectors and  $\|\cdot\|$  the norm of a vector. The equation for the projection vector  $\vec{Pr}j_b(t)$  of vector  $\vec{P}'_b(t)$  on the vector  $\vec{U}(t)$  is similar. Subtracting the projection vectors and using the fact that the inner product is bilinear, we have that

$$\vec{Pr}j_a(t) - \vec{Pr}j_b(t) = \frac{\langle \vec{P}'_a(t) - \vec{P}'_b(t), \vec{U}(t) \rangle}{\|\vec{U}(t)\|} \cdot \frac{\vec{U}(t)}{\|\vec{U}(t)\|}. \quad (8)$$

Let  $v(t)$  be the relative velocity (m/s) between a transmitter and a receiver at time  $t$ . Let  $c$  be the signal propagation speed (m/s). At nominal frequency  $f_0$  Hz, the Doppler effect causes a frequency shift defined as

$$f_{\Delta}(t) = f_0 \frac{v(t)}{c} \text{ Hz}. \quad (9)$$

Using Equations (8) and (9), we derive the Doppler effect resulting from the movement of two vehicles in Theorem 1.

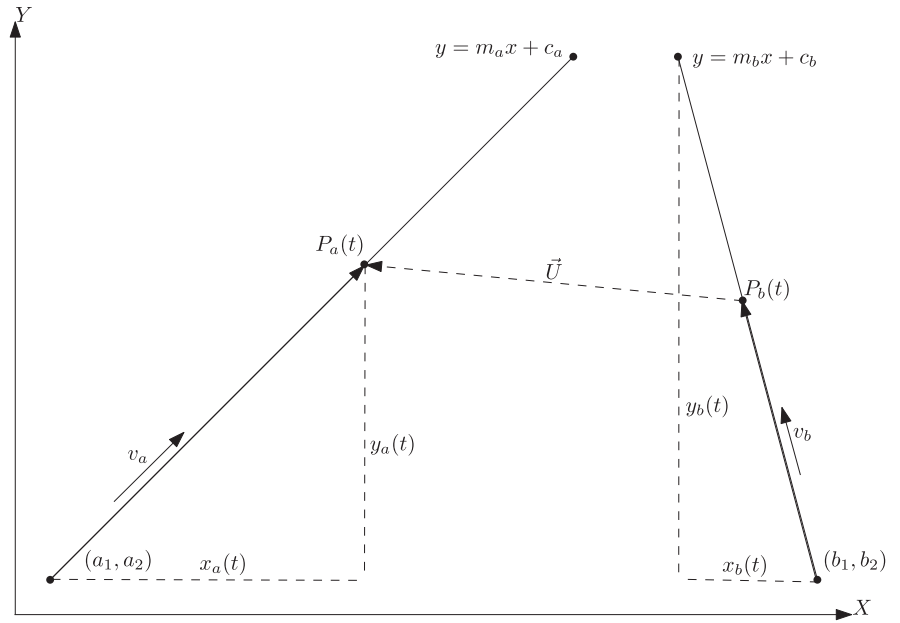


**FIGURE 3** In the Euclidean plane, the motions of vehicles  $R_a$  and  $R_b$  along straight-line trajectories modeled by the Cartesian equations  $y = m_a x + c_a$  and  $y = m_b x + c_b$

**Theorem 1** (Doppler effect). For two vehicles  $R_a$  and  $R_b$  moving in the Euclidean space with constant velocities  $v_a$  and  $v_b$  on their respective straight-line trajectories defined by the mappings  $t \rightarrow \vec{P}_a(t)$  and  $t \rightarrow \vec{P}_b(t)$ , the change in frequency due to the Doppler effect is

$$\Delta f(t) = -\text{sign}(\|\vec{U}(t)\|') \cdot \frac{\left| \langle \vec{P}'_a(t) - \vec{P}'_b(t), \vec{U}(t) \rangle \right|}{\|\vec{U}(t)\|} \cdot \frac{f_0}{c}, \quad (10)$$

where  $|\cdot|$  denotes the absolute value,  $f_0$  the transmission frequency, and  $c$  the underwater sound speed.

Note that the evaluation of the term  $-\text{sign}(\|\vec{U}(t)\|')$  is positive when the projections of the colinear vectors  $\vec{P}'_a(t)$  and  $\vec{P}'_b(t)$  are pointing towards each other and negative when they are in opposite directions.

Consider two vehicles  $R_a$  and  $R_b$  moving along trajectories defined by the straight lines  $t \rightarrow \vec{P}_a(t) := \vec{A}t + a$  and  $t \rightarrow \vec{P}_b(t) := \vec{B}t + b$ , where  $a, b, \vec{A}, \vec{B}$  are constants initial positions and velocity vectors in the Euclidean plane. The initial positions of the vehicles are  $P_a(0) = a$  and  $P_b(0) = b$ . We can derive the following. Given the equivalences

$$\vec{P}'_a(t) = \vec{A}, \vec{P}'_b(t) = \vec{B} \text{ and } \vec{U}(t) = (\vec{B} - \vec{A})t + b - a, \quad (11)$$

we have that

$$\|\vec{U}(t)\| = \sqrt{\sum_{i=1}^2 [(B_i - A_i)t + (b_i - a_i)]^2}. \quad (12)$$

Applying the rule  $du^{\frac{1}{2}}/dx = 1/2 \cdot u^{-\frac{1}{2}} \cdot du/dx$ , we get

$$\|\vec{U}(t)\|' = \frac{\sum_{i=1}^2 [(B_i - A_i)t + (b_i - a_i)] \cdot (B_i - A_i)}{\sqrt{\sum_{i=1}^2 [(B_i - A_i)t + (b_i - a_i)]^2}}. \quad (13)$$

Substituting these formulas into Equation (10), we can determine the equation for the change in frequency  $f_{\Delta}(t)$  as measured by the Doppler effect in Theorem 1. We summarize this in the Corollary 1.

**Corollary 1.** Given two vehicles  $R_a$  and  $R_b$ , with initial positions  $a, b$  and velocity vectors  $\vec{A}, \vec{B}$ , as a function of time  $t$ , the Doppler shift is

$$f_{\Delta}(t) = -\text{sign} \left( \sum_{i=1}^2 [(B_i - A_i)t + (b_i - a_i)] \cdot (B_i - A_i) \right) \cdot \frac{|\langle \vec{A} - \vec{B}, (\vec{B} - \vec{A})t + b - a \rangle|}{\sqrt{\sum_{i=1}^2 ((B_i - A_i)t + (b_i - a_i))^2}} \cdot \frac{f_0}{c}, \quad (14)$$

where  $f_0$  is the transmission frequency and  $c$  the underwater sound speed.

### 3.2 | Normalizer

During the frame search procedure, the carrier of the signal can be tracked assuming trajectory parameters instantiating Equation (14). For vehicles  $R_a$  and  $R_b$ , an actualization of the parameters consists of the following trajectory pair:

$$\mathcal{T} = [(a, m_a, c_a, v_a), (b, m_b, c_b, v_b)]. \quad (15)$$

Several plausible combinations of values for the eight parameters contained in  $\mathcal{T}$  can be tried to tune in the correct Doppler effect. However, it can be observed that several instances of Equation (14), with different parameters, yield exactly the same Doppler effect, represented by  $f_{\Delta}(t)$ . This is consistent with the fact that the Doppler effect pattern is relative to a sender-receiver velocity, see Equation (9), and their relative initial separation distance. Several different configurations may result into equivalent Doppler effects. Hence, the search space can be greatly reduced by normalizing the trajectories and trying only one representative per equivalence class.

For example, let us place stationary vehicle  $R_a$  at the origin and place mobile vehicle  $R_b$  at the initial position  $p$  with constant velocity vector  $\vec{V}$ . Figure 4 depicts four different cases for initial position  $p$  and velocity vector  $\vec{V}$ . Corresponding to length between the origin and point  $p$ , the relative distance is always the same. The magnitude of the projection of  $\vec{V}$  on a line through the origin and  $p$  is always the same, as well as its orientation relative to the origin (facing or opposite). The bottom-right case can be chosen as the representative for all the equivalent four cases, w.r.t. the Doppler effect. In each of the first three case, the arc represents a rotation that is applied to point  $p$  to make it equivalent to the fourth case.

Normalization of trajectories is defined with respect to the resulting Doppler effect. Firstly, a position of a vehicle, let us say  $R_a$ , is made the center of the coordinate system. The position of the second vehicle, ie,  $R_b$ , is expressed relative to

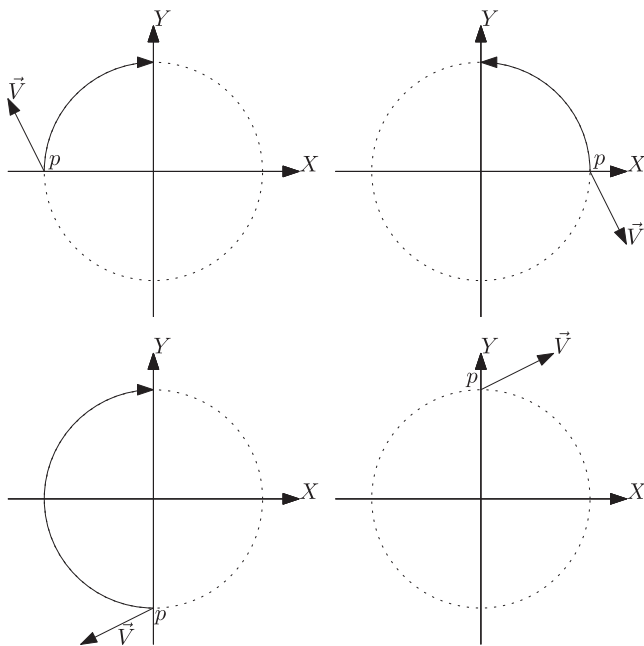


**FIGURE 4** Equivalence due to same relative initial distance and magnitude of projection of velocity vector  $\vec{V}$  on an axis through the origin and point  $p$ , w.r.t. the Doppler effect



the origin of the coordinate system. Given the initial positions  $a$  and  $b$  of  $R_a$  and  $R_b$ , centering  $R_a$  at the origin, the relative initial position of  $R_b$  is a new point

$$p = b - a. \quad (16)$$

Secondly, velocities can be expressed relative to one of the vehicles. In other words, one vehicle is stationary, and the other is relatively moving. Let  $\vec{A}$  and  $\vec{B}$  be the velocity vectors of  $R_a$  and  $R_b$ . Making  $R_a$  stationary relative to  $R_b$ , the relative velocity of  $R_b$  becomes a new vector

$$\vec{V} = \vec{B} - \vec{A}. \quad (17)$$

Thirdly, the position  $p$  can be expressed in a coordinate system in which its direction is always the same, relative to  $R_b$ . For example,  $p$  can be placed on the positive  $Y$ -axis. In such a case, the first coordinate of  $p$ , ie,  $p_1$ , is always null. Fourthly, to remove redundancy due to symmetry, the absolute value of the first component of  $\vec{V}$  is taken, ie,  $\vec{V}$  equal to  $(v_1, v_2)$  is mapped to  $(|v_1|, v_2)$ . The transformations of  $p$  and  $\vec{V}$  can be done consistently with a rotation matrix. These ideas are formalized in Theorem 2.

**Theorem 2.** *Let the vehicle  $R_a$  be positioned at the center of the coordinate system. Let the vehicle  $R_b$  be positioned at relative position  $p$  with relative velocity vector  $\vec{V}$ . Vector  $\vec{V}$  and initial position  $p$  can be rotated around a circle centered at the origin and radius equal to  $\|p\|$  while producing identical Doppler effect at  $R_a$ .*

*Proof.* The Doppler effect depends on the relative velocity of vehicle  $R_b$  with respect to vehicle  $R_a$ , cf, Equation (9). This relative velocity can be obtained by the scalar projection of  $\vec{V}$  onto  $p$

$$s = \frac{\langle \vec{V}, p \rangle}{\|p\|}.$$

We show that  $s$  is invariant to the application of a rotation by  $\theta$  degrees. In the Euclidean plane, a clockwise vector rotation of an angle  $\theta$  is defined by the rotation matrix

$$R(\theta) = \begin{bmatrix} \cos \theta & \sin \theta \\ -\sin \theta & \cos \theta \end{bmatrix}.$$

Note that  $\|p\|$ , the distance between point  $p$  and the origin, is invariant. It is also true for the dot product

$$\langle R(\theta)\vec{V}', R(\theta)p \rangle = \langle \vec{V}R(-\theta), R(\theta)p \rangle = \langle \vec{V}, p \rangle. \quad \square$$

Redundancy due to symmetry is captured in Theorem 3.

**Theorem 3.** *Let the vehicle  $R_a$  be positioned at the center of the coordinate system. Let the vehicle  $R_b$  be positioned on the  $Y$ -axis at relative coordinated  $p$  equal to  $(0, p_2)$  and with relative velocity vector  $\vec{V}$  equal to  $(V_1, V_2)$  mapped to  $(|V_1|, V_2)$ . Vector  $\vec{V}$  is mapped to  $(|V_1|, V_2)$  while producing identical Doppler effect at  $R_a$ .*

*Proof.* We have the following equivalences  $\langle (V_1, V_2), (0, p_2) \rangle = \langle (-V_1, V_2), (0, p_2) \rangle = \langle (|V_1|, V_2), (0, p_2) \rangle. \quad \square$

During the frame search procedure, we try directly ranges of values for the pairs  $(p, \vec{V})$ , where  $p$  is a position on the positive  $Y$ -axis and  $\vec{V}$  is a velocity vector ( $p_1 = 0$  and  $V_1 > 0$ ), and apply Corollary 2.

**Corollary 2.** *Let us consider a stationary vehicle  $R_a$ , placed at the origin of the coordinate system, and a mobile vehicle  $R_b$ , with initial position  $p$ , with  $p_1$  equal to zero,  $p_2 \geq 0$  and velocity vectors  $\vec{V}$ , with first component  $V_1$  a positive number. As a function of time  $t$ , the Doppler shift is*

$$f_{\Delta}(t) = -\text{sign} \left( \sum_{i=1}^2 (V_i t + p_i) \cdot V_i \right) \cdot \frac{|\langle \vec{V}, \vec{V}t + p \rangle|}{\sqrt{\sum_{i=1}^2 (V_i t + p_i)^2}} \cdot \frac{f_0}{c}, \quad (18)$$

where  $f_0$  is the transmission frequency and  $c$  is the underwater sound speed.



## 4 | INTEGRATION OF NORMALIZED TRAJECTORY MODEL INTO THE DEMODULATOR DESIGN

We revisit the demodulator design described in the work of Barbeau,<sup>11</sup> integrating the concept of normalized trajectory. The original design builds upon ideas authored by Taylor and Walker,<sup>51</sup> Franke and Taylor,<sup>52</sup> Karn,<sup>53</sup> and Fano.<sup>54</sup> The integration of the normalized trajectory model extends the original design with the capability to efficiently look for frames with possibly linearly or nonlinearly drifting carriers.

We briefly outline the challenges presented by underwater communications. The highlights of the communication protocol on which the modem design is based are discussed. Finally, we detail the integration of the notion of normalized trajectory into the demodulator design.

### 4.1 | Underwater communication

Underwater communication uses sound waves. Significant communication impairments include attenuation and numerous sources of noise.<sup>6</sup> For long-range communication, attenuation is an important issue. It is due to conversion of acoustic energy into heat and geometrical spreading. Its importance grows with distance and frequency. Hence, for long distances, solely the use of low frequencies can be envisioned. Another important fact is the gradient of the attenuation versus frequency. It limits the operating bandwidth. The half-power bandwidth is commonly used to define cutoff frequencies and bandwidths of filters by using frequency response curves, using 3 dB points in the frequency response of a band-pass filter.<sup>55</sup> At low frequency (in the few kHz range), attenuation is low relative to higher frequencies (eg, 20 kHz), but the gradient of the attenuation is high. Consequently, the half-power bandwidth is very narrow, ie, just a few Hz. Solely narrow-band modulation is possible, ie, a few Hz.

### 4.2 | Communication protocol

The protocol used by the demodulator is asynchronous frame-oriented. Each frame comprises 162 channel symbols that encode 50 information bits. Convolutional forward error correction is used, with a constraint of 32 and a rate of 1/2.<sup>54</sup> Convolutional encoding of the information bits yields 162 bits. They are interleaved with 162 synchronization bits  $s_i$  ( $i = 0, \dots, 161$ ). Every data bit is paired with a synchronization bit. Each pair makes a channel symbol. Modulation is 4-FSK at 1.46 (375/256) baud. The complex modulation envelope frequencies are  $-2.2$ ,  $-0.7$ ,  $0.7$ , and  $2.2$  Hz, corresponding to channel symbols 0, 1, 2, and 3. The signal bandwidth is therefore 4.4 Hz. The transmission time of a frame is 111 seconds.

### 4.3 | Normalized trajectory model integration

The demodulator captures the audio with a hydrophone. The analog signal is digitized, band pass filtered, and centered to zero Hz. Digitized audio processing is done following a sliding window on buffered samples. Each window spans 120 seconds of samples. The next window is slid 9 seconds in time. The discrete complex samples of a window are denoted  $x_0, x_1, \dots, x_{n-1}$ , with  $n$  equal to 45 000. Therefore, the sampling rate  $f_s$  is equal to the ratio  $n/120 = 375$  samples per second (sps). Each channel symbol consists of 256 samples. A frame comprises 256 samples per symbol times 162 channel symbols, ie, a total of 41 472 samples.

Each window of channel data is searched for the presence of 111-second frames. Windowed fast Fourier transforms (FFTs) are calculated. Each FFT represents a time interval corresponding to the duration of two symbols, ie, 512 samples. The size  $N$  of each FFT is 512 bins.\* The FFTs are calculated from the beginning of a 2-minute interval, in steps of half symbol (128 samples). The number of FFTs, denoted as  $n_{\text{ffts}}$ , is equal to  $\lfloor n/128 \rfloor - 3 = 348$  FFTs. The subtrahend 3 is present because calculations of windowed FFTs stop before the third to last half-sample. According to Nyquist criterion, at 375 sps, the frequency range of each FFT is lower than  $375/2$  Hz, ie, including the negative frequencies within the range  $\pm 187$  Hz. From frequency-bin-to-frequency-bin, there is an offset  $\Delta f$  of  $375/512 = 0.73$  Hz. Every FFT coefficient is defined as

$$X_{m,k} = \sum_{t=0}^{N-1} x_{128m+t} \cdot w(t) \cdot e^{-j2\pi kt/N}. \quad (19)$$

\*When conducting discretization of frequencies, we get frequency bins, ie, the continuous frequencies become  $N$  discrete bins.<sup>56</sup>

The FFT window index  $m$  is in the range  $0, \dots, \text{nffts} - 1$ . The windowing function  $w(t)$  is defined as  $\sin(\pi t/512)$ . Equation (19) represents the relative amplitude and phase of frequency

$$\frac{k \cdot f_s \text{ sps}}{N \text{ samples}} \text{ Hz.}$$

Because there are 512 bins, the coefficient index  $k$  is in the range  $-256, \dots, -1, 0, \dots, 255$ . In the frequency domain, every 2-minute time interval is represented by the following matrix:

$$X = \begin{pmatrix} X_{0,-256} & \dots & X_{0,0} & \dots & X_{0,255} \\ \vdots & \dots & \vdots & \dots & \vdots \\ X_{\text{nffts}-1,-256} & \dots & X_{\text{nffts}-1,0} & \dots & X_{\text{nffts}-1,255} \end{pmatrix}. \quad (20)$$

The frequency domain representation is used for a coarse signal search. The procedure looks for candidates in the frequency domain, ie, columns in matrix (20), where there is a local signal-to-noise ratio (SNR) maximum, see the work of Barbeau.<sup>11</sup> Using the corresponding frequencies as candidate carriers, refined signal paths are searched. A path is defined by a signal tracking function  $f_\theta : \{0 \dots \text{nffts} - 1\} \mapsto \{-256 \dots 0 \dots 255\}$ , where  $\theta$  is a parameter of  $f$ . Let  $\Phi$  denote the set of all instances of such signal tracking functions (assume it is finite size, ie, there is a finite number of functions and the domains of their parameters are finite).

Next, we consider three cases depending on how tracking of the signal is influenced by the Doppler effect.

*Case 1.* Tracking of a signal not subject to the Doppler effect, ie, its frequency is not drifting, is represented by a constant function  $f(i) = c$ , where  $i$  is the half-symbol index and  $c$  is the carrier frequency.

*Case 2.* Tracking of a signal subject to a Doppler effect such that the carrier frequency is drifting linearly is represented by function  $f_\delta(i)$  equal to  $c + \delta i$ . The parameter  $\delta$  represents the quantity of frequency drift per half-symbol.

*Case 3.* Tracking of a signal subject to a Doppler effect such that the carrier frequency is drifting nonlinearly is represented by an arbitrary function. The total number of possible signal tracking function is  $N^{\text{nffts}}$ , ie, exponential.

Handling of Cases 1 and 2 has been discussed in previous works. The contribution in this article is about Case 3. A strategy is proposed to avoid an exponential search. We build upon the work described in Section 3. The parameter  $\theta$  of the signal tracking function  $f_\theta$  is a normalized trajectory represented by a pair  $(p, \vec{V})$ . The first component of the initial position  $p$ , ie,  $p_1$ , is zero. For the second component, ie,  $p_2$ , a range of distances from  $d_{\min}$  to  $d_{\max}$ , in steps of  $d_{\text{step}}$ , is explored. For the velocity vector  $\vec{V}$ , a range of angles between  $a_{\min}$  to  $a_{\max}$ , in steps of  $a_{\text{step}}$ , together with a range of magnitudes  $m_{\min}$  to  $m_{\max}$ , in steps of  $m_{\text{step}}$ , is tried. The time complexity of this search is cubic. Note that because they generate constant frequency drifts, we skip cases when the velocity vector is colinear with y-axis and positive or when the velocity vector is colinear with y-axis, negative, and vehicle does not cross x-axis during a frame reception (due to long distance or slow velocity).

For each candidate signal, defined by a signal tracking function  $f_\theta$ , this step finds a coarse time offset, from the start of a two minute interval. Each candidate signal is examined. A complete frame can start anywhere from the beginning to a time delay corresponding to nine seconds (26 half-symbols) into the interval. Let  $W_{m,k} = |X_{m,k}|$  denote the magnitude spectrum at indices  $m$  and  $k$ . For the signal tracking function  $f_\theta$ , the timing offset  $\tau$  is the value in the range  $0, \dots, 25$  that maximizes the sum

$$\sum_{i=0}^{161} (2s_i - 1) \left[ \frac{(W_{2i+\tau, f_\theta(2i+\tau)-4} + W_{2i+\tau, f_\theta(2i+\tau)+1}) - (W_{2i+\tau, f_\theta(2i+\tau)-1} + W_{2i+\tau, f_\theta(2i+\tau)+4})}{\sum_{k=-4, -1, 1, 4} |W_{2i+\tau, f_\theta(i)+k}|} \right].$$

The summation measures the correlation of the spectrum power around the frequency returned by the function  $f_\theta$  with the synchronization bit-string  $s$ . The multiplicand  $2s_i - 1$  maps the synchronization bit  $s_i$ , which is 0 or 1, to value  $-1$  or  $1$ . The term  $W_{2i+\tau, f_\theta(2i+\tau)-4} + W_{2i+\tau, f_\theta(2i+\tau)+1}$  is the sum of the magnitudes at the frequencies of synchronization bit value  $1$ , while the term  $W_{2i+\tau, f_\theta(2i+\tau)-1} + W_{2i+\tau, f_\theta(2i+\tau)+4}$  is the sum of the magnitudes at the frequencies of synchronization bit

value 0. The denominator represents the sum of all magnitudes around frequency  $f_\theta(i)$ . The power at synchronization bits is made relative to all the power at the candidate frequency.

For each signal tracking function  $f_\theta$ , over a symbol interval of length  $T$ , the signal samples correlated with the waveforms are added to obtain the total magnitude at each symbol frequency ( $f = -2.2, -0.7, 0.7, 2.2$ )

$$P_{i,f} = \left| \sum_{t=iT+\tau}^{(i+1)T+\tau} x_t \cdot e^{-j2\pi[f_\theta(t)-0.73+f]t} \right|. \quad (21)$$

The list of four magnitudes  $P_{i,f}$  are used to calculate soft symbols. A soft symbol represents a value and its quality. Receive quality metrics are associated with the symbols. This information is used in the decoding process. The most likely symbols are selected first. A de-interleaving procedure reorders the 162 data soft symbols. The resulting 162 soft symbols are passed to a forward error correction decoder.

## 5 | PERFORMANCE

The performance of the demodulator has been evaluated through simulation and experimentation. Figure 5 plots the frame error rate (FER) as a function of the SNR for a baseline theoretical performance (without Doppler handling), our modem design (with Doppler handling) and other underwater modem designs. A frame is considered correct when it is received free of errors. For our modem design, we use performance data from our previous publications.

For reference purposes, the theoretical performance of 4-FSK noncoherent demodulation is plotted, using the bit error rate (BER) versus SNR per bit model in the work of Massoud Salehi and Proakis.<sup>57</sup> We refer to these curves as the theoretical curve with the term *Baseline (without Doppler)*. The SNR per bit, also called the energy per bit to noise power spectral density ratio ( $E_b/N_0$ ), is related to the SNR

$$\text{SNR} = \frac{E_b R}{N_0 B}. \quad (22)$$

$R$  denotes the data rate and  $B$  the channel bandwidth. As for our modem design, we use a data rate of 0.45 bps and a reference bandwidth of 2.5 kHz to calculate the SNR. The theoretical performance is a baseline reference. It takes into account solely white noise and not, for instance, the Doppler effect. We do not expect our design to do better than the theoretical performance. However, the performance of our modem design is approaching the theoretical performance. It is well known that this can be achieved with high redundancy FEC, 300% in our case.

Since the data frames in our modem design are 50-bit long, the theoretical BER is converted to a FER using the following equation:

$$\text{FER} = 1 - (1 - \text{BER})^{50}. \quad (23)$$

Given the BER, it is the probability of receiving an error-free 50-bit frame.

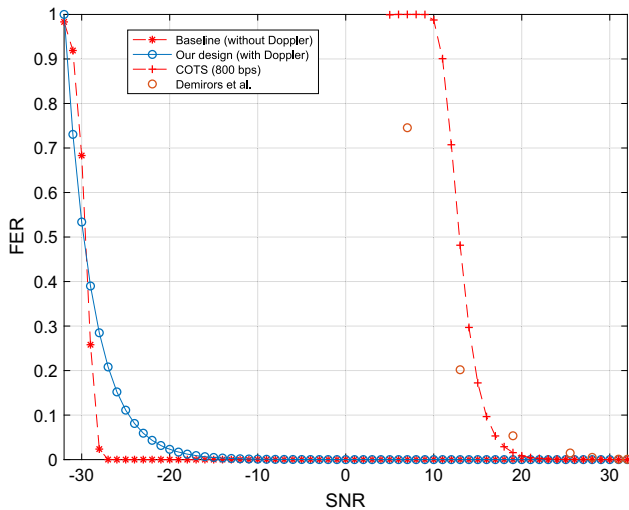
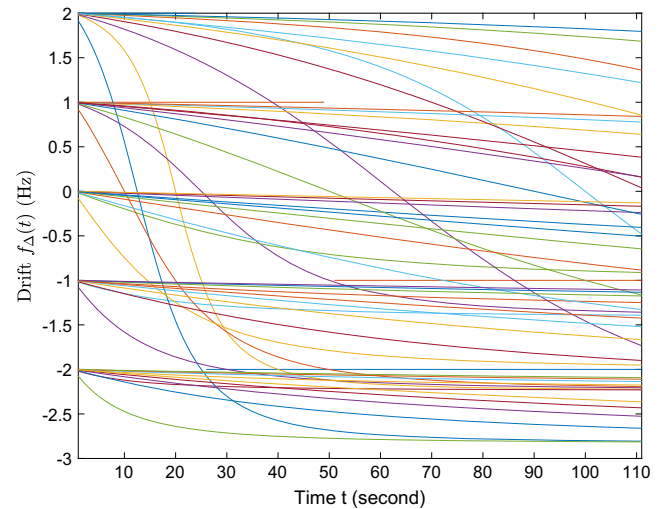


FIGURE 5 Frame error rate (FER) vs signal-to-noise ratio (SNR)



**FIGURE 6** Doppler patterns produced by a range of values for normalized trajectories

For our modem design, the curve has been derived fitting data points obtained through a simulation.<sup>9</sup> A reference bandwidth of 2.5 kHz is used to calculate the SNR, corresponding to the bandwidth of a single-sideband audio channel. The demodulator starts performing with a SNR above  $-25$  dB, yielding a FER of 10% and below.

In Figure 5, we compare our underwater modem design performance using the best BER model obtained during the sea trial documented in table 2 in the work by Blouin,<sup>58</sup> rate 800 (bps). The data had been obtained with a commercial off-the-shelf underwater acoustic modem at 800 bps. The BER model is converted to a FER using Equation (23). We also compare with the best performance results documented in the work of Demirors et al.,<sup>31</sup> quadrature phase shift keying, no coding, 104 kbit/s, at 90 m. The FER data points are also converted to FER data points using Equation (23). With respect to these two modem designs, our modem design can operate under much lower SNR conditions. The trade-offs are, of course, an extremely low data rate and delays due to the off-line nature of the frame search strategy used in our modem design.

Figure 6 plots frequency drift patterns due to the Doppler effect for a range of normal trajectories. For this example, the nominal frequency is 1.5 kHz. The relative distance of the initial position varies from 50 to 850 m in steps of 200 m. For the relative velocity vectors, all combinations of horizontal velocity from 0 to 2 m/s and vertical velocity from  $-2$  to 2 m/s (both in steps of 1 m) are plotted. Every Doppler shift curve is unique. The normalized trajectory model described in this paper does not affect the previous FER vs SNR performance. However, the normalization strategy eliminates checking redundant Doppler patterns during the search for frames. In Section 3.2, we demonstrate the theoretical validity of this improvement. Note, however, that the gain in performance is application specific and depends on the actual sets of trajectory parameters that are considered, in particular the end of Section 5.

## 6 | CONCLUSION

We have developed a demodulator design for low-frequency underwater acoustic communication to address arbitrary Doppler shift patterns identified in our previous works.<sup>8,9</sup> The demodulator design handles nonlinearly variable Doppler shifts under the assumption that it can be attributed to a normalized straight-line trajectory model. With respect to the initial version of this work,<sup>10</sup> we have introduced a normalizer concept that eliminates redundant Doppler effect patterns during the frame search process. Our work has also been validated theoretically, for the normalization aspect, and experimentally, for the communication aspect. The results of the experiment are described in companion papers.<sup>11,58</sup> More mathematical, implementation details, source code, and examples are available in other works<sup>8-11,59,60</sup> and online at [github.com/michelbarbeau/gr-uwspr](https://github.com/michelbarbeau/gr-uwspr).

## ACKNOWLEDGMENTS

Work partially supported by the Natural Sciences and Engineering Research Council of Canada (NSERC) and the European Commission under grant agreement 830892 (H2020 SPARTA project).

## ORCID

Michel Barbeau  <https://orcid.org/0000-0003-3531-4926>

Joaquin Garcia-Alfaro  <https://orcid.org/0000-0002-7453-4393>

Evangelos Kranakis  <https://orcid.org/0000-0002-8959-4428>

## REFERENCES

- Otnes R, Voldhaug JE, Haavik S. On communication requirements in underwater surveillance networks. In: Proceedings of the OCEANS 2008-MTS/IEEE Kobe Techno-Ocean; 2008; Kobe, Japan.
- Otnes R, Asterjadhi A, Casari P, et al. *Underwater Acoustic Networking Techniques*. Heidelberg, Germany: Springer Science & Business Media; 2012.
- Button RW, Kamp J, Curtin TB, Dryden J. A survey of missions for unmanned undersea vehicles. Santa Monica, CA: RAND National Defense Research Institute; 2009. <https://apps.dtic.mil/docs/citations/ADA503362>. Accessed February 25, 2019.
- Decarpigny JN, Hamonic B, Wilson OB. The design of low frequency underwater acoustic projectors: present status and future trends. *IEEE J Ocean Eng*. 1991;16(1):107-122.
- Hixson E. A low-frequency underwater sound source for seismic exploration. *J Acoust Soc Am*. 2009;126(4):2234.
- Stojanovic M. On the relationship between capacity and distance in an underwater acoustic communication channel. *SIGMOBILE Mob Comput Commun Rev*. 2007;11(4):34-43.
- Freitag L, Ball K, Partan J, Koski P, Singh S. Long range acoustic communications and navigation in the arctic. In: Proceedings of the OCEANS 2015-MTS/IEEE Washington; 2015; Washington, DC.
- Ahmad A-M, Barbeau M, Garcia-Alfaro J, Kassem J, Kranakis E, Porretta S. Doppler effect in the underwater acoustic ultra low frequency band. In: *Ad Hoc Networks: 9th International Conference, AdHocNets 2017, Niagara Falls, ON, Canada, September 28-29, 2017, Proceedings*. Cham, Switzerland: Springer International Publishing; 2018:3-12.
- Ahmad A-M, Kassem J, Barbeau M, Kranakis E, Porretta S, Garcia-Alfaro J. Doppler effect in the acoustic ultra low frequency band for wireless underwater networks. *Mob Netw Appl*. 2018;23(5):1282-1292. <https://doi.org/10.1007/s11036-018-1036-9>. Accessed February 25, 2019.
- Ahmad AM, Barbeau M, Garcia-Alfaro J, Kassem J, Kranakis E, Porretta S. Low frequency mobile communications in underwater networks. In: *Ad-hoc, Mobile, and Wireless Networks: 17th International Conference on Ad Hoc Networks and Wireless, ADHOC-NOW 2018, Saint-Malo, France, September 5-7, 2018, Proceedings*. Cham, Switzerland: Springer; 2018:239-251.
- Barbeau M. Weak signal underwater communications in the ultra low frequency band. In: Proceedings of the 7th GNU Radio Conference; 2017; San Diego, CA. <https://pubs.gnuradio.org/index.php/grcon/article/view/20/14>. Accessed February 25, 2019.
- Sharif BS, Neasham J, Hinton OR, Adams AE. A computationally efficient Doppler compensation system for underwater acoustic communications. *IEEE J Ocean Eng*. 2000;25(1):52-61.
- Li B, Zhou S, Stojanovic M, Freitag L, Willett P. Multicarrier communication over underwater acoustic channels with nonuniform Doppler shifts. *IEEE J Ocean Eng*. 2008;33(2):198-209.
- Wu L, Trezzo J, Mirza D, et al. Designing an adaptive acoustic modem for underwater sensor networks. *IEEE Embed Syst Lett*. 2012;4:1-4.
- Ming L, Lin Z, Yide Z. A novel Doppler frequency shift compensation algorithm for OFDM underwater acoustic communication system. In: Proceedings of the 25th Chinese Control and Decision Conference (CCDC); 2013; Guiyang, China.
- Kim YH, Song I, Yoon S, Park SR. An efficient frequency offset estimator for OFDM systems and its performance characteristics. *IEEE Trans Veh Technol*. 2001;50(5):1307-1312.
- Antonelli G. *Underwater Robots*. Cham, Switzerland: Springer International Publishing; 2018. *Springer Tracts in Advanced Robotics*.
- lanbo L, Shengli Z, Jun-Hong C. Prospects and problems of wireless communication for underwater sensor networks. *Wirel Commun Mob Comput*. 2008;8:977-994.
- Lanzagorta M. *Underwater Communications*. 1st ed. San Rafael, CA: Morgan & Claypool; 2013. *Synthesis Lectures on Communications*; vol. 6.
- Zhou S, Wang Z. *OFDM for Underwater Acoustic Communications*. Chichester, UK: John Wiley & Sons; 2014.
- Stojanovic M, Preisig J. Underwater acoustic communication channels: propagation models and statistical characterization. *IEEE Commun Mag*. 2009;47(1):84-89.
- Mitola J. *Software Radio Architecture: Object-Oriented Approaches to Wireless Systems Engineering*. New York, NY: John Wiley & Sons; 2004.
- Dillinger M, Madani K, Alonistioti N. *Software Defined Radio: Architectures, Systems and Functions*. Chichester, UK: John Wiley & Sons; 2005.
- The GNU Radio Foundation, Inc. GNU Radio: The Free and Open Software Radio Ecosystem. 2019. <https://www.gnuradio.org>. Accessed February 25, 2019.
- Dol HS, Casari P, van der Zwan T, Otnes R. Software-defined underwater acoustic modems: Historical review and the NILUS approach. *IEEE J Ocean Eng*. 2017;42(3):722-737.
- Borowski B, Duchamp D. The softwater modem: a software modem for underwater acoustic communication: short paper. In: Proceedings of the Fourth ACM International Workshop on Underwater Networks; 2009; Berkeley, CA.



27. Demirors E, Sklivanitis G, Melodia T, Batalama SN, Pados DA. Software-defined underwater acoustic networks: toward a high-rate real-time reconfigurable modem. *IEEE Commun Mag.* 2015;53(11):64-71.
28. Cario G, Casavola A, Lupia M, Rosace C. SeaModem: a low-cost underwater acoustic modem for shallow water communication. In: Proceedings of the OCEANS 2015 - Genova; 2015; Genova, Italy.
29. Benson B, Li Y, Faunce B, et al. Design of a low-cost underwater acoustic modem. *IEEE Embed Syst Lett.* 2010;2(3):58-61.
30. Goncalves MA, Louredo RV, Tcheou MP, Lovisolio L. Acoustic modem using OFDM and least-square channel estimation. In: Proceedings of the 2017 IEEE 9th Latin-American Conference on Communications (LATINCOM); 2017; Guatemala City, Guatemala.
31. Demirors E, Sklivanitis G, Santagati GE, Melodia T, Batalama SN. A high-rate software-defined underwater acoustic modem with real-time adaptation capabilities. *IEEE Access.* 2018;6:18602-18615.
32. Huang X, Lawrence VB. OFDM with pilot aided channel estimation for time-varying shallow water acoustic channels. In: Proceedings of the 2010 International Conference on Communications and Mobile Computing; 2010; Caen, France.
33. Chen Y, Zou L, Zhao A, Yin J. Null subcarriers based Doppler scale estimation for multicarrier communication over underwater acoustic non-uniform Doppler shift channels. In: Proceedings of the 2016 IEEE/OES China Ocean Acoustics (COA); 2016; Harbin, China.
34. Huang Y, Wang Z, Zhou S. Characterization and receiver design for underwater acoustic channels with large Doppler spread. In: Proceedings of the Oceans 2015 - MTS/IEEE Washington; 2015; Washington, DC.
35. Amar A, Avrashi G, Stojanovic M. Low complexity residual Doppler shift estimation for underwater acoustic multicarrier communication. *IEEE Trans Signal Process.* 2017;65(8):2063-2076.
36. Jing L, He C, Huang J, Ding Z. Joint channel estimation and detection using Markov chain Monte Carlo method over sparse underwater acoustic channels. *IET Communications.* 2017;11(11):1789-1796.
37. Li C, Song K, Yang L. Low computational complexity design over sparse channel estimator in underwater acoustic OFDM communication system. *IET Communications.* 2017;11(7):1143-1151.
38. Lu Q, Hu X, Wang D, Zhou S. Parallel combinatory multicarrier modulation in underwater acoustic communications. *IET Communications.* 2017;11(9):1331-1337.
39. Zhang X, Song K, Li C, Yang L. Parameter estimation for multi-scale multi-lag underwater acoustic channels based on modified particle swarm optimization algorithm. *IEEE Access.* 2017;5:4808-4820.
40. Yu X, Wang Y, Guan X. Doppler scale estimation for underwater acoustic communications using dual Zadoff-Chu sequences. In: Proceedings of the 2018 IEEE International Conference on Signal Processing, Communications and Computing (ICSPCC); 2018; Qingdao, China.
41. Hou Z, Zhou Y, Tian L, Shi J, Li Y, Vucetic B. Radio environment map-aided Doppler shift estimation in LTE railway. *IEEE Trans Veh Technol.* 2017;66(5):4462-4467.
42. Huang S, Fang S, Han N. Parameter estimation of delay-Doppler underwater acoustic multi-path channel based on iterative fractional Fourier transform. *IEEE Access.* 2019;7:7920-7931.
43. Abougamila S, Elmorsy M, Elmallah ES. On probabilistic connected components in underwater sensor networks. In: Proceedings of the 2018 IEEE 43rd Conference on Local Computer Networks (LCN); 2018; Chicago, IL.
44. Bouabdallah F. Time evolution of underwater sensor networks coverage and connectivity using physically based mobility model. *Wirel Commun Mob Comput.* 2019;2019.
45. Heidemann J, Stojanovic M, Zorzi M. Underwater sensor networks: applications, advances and challenges. *Philos Trans Math Phys Eng Sci.* 2012;370:158-175.
46. Jones C, Morozov A, Manley JE. Under ice positioning and communications for unmanned vehicles. In: Proceedings of the 2013 MTS/IEEE OCEANS-Bergen; 2013; Bergen, Norway.
47. Dong Q, Wang Y, Guan X. The design and implementation of an underwater multimode acoustic modem for autonomous underwater vehicles. In: Proceedings of the 2018 37th Chinese Control Conference (CCC); 2018; Wuhan, China.
48. Bernaldo de Quirós Y, Fernandez A, Baird RW, et al. Advances in research on the impacts of anti-submarine sonar on beaked whales. *Proc Royal Soc B.* 2019;286.
49. Li X, Sun Y, Guo Y, Fu X, Pan M. Dolphins first: dolphin-aware communications in multi-hop underwater cognitive acoustic networks. *IEEE Trans Wirel Commun.* 2017;16(4):2043-2056.
50. McCartney BS. Underwater acoustic positioning systems: state of the art and applications in deep water. *Int Hydrogr Rev.* 1981;58(1):91-113.
51. Taylor J, Walker B. WSPRing around the world. *QST.* 2010;94(10):30-32.
52. Franke S, Taylor J. WSPR. 2019. <http://physics.princeton.edu/pulsar/K1JT/wspr.html>. Accessed February 25, 2019.
53. Karn P. Convolutional decoders for amateur packet radio. In: Proceedings of the ARRL Digital Communications Conference; 1995; Arlington, TX.
54. Fano R. A heuristic discussion of probabilistic decoding. *IEEE Trans Inf Theory.* 1963;9(2):64-74.
55. Wu B. A correction of the half-power bandwidth method for estimating damping. *Arch Appl Mech.* 2015;85:315-320.
56. Harris FJ. On the use of windows for harmonic analysis with the discrete Fourier transform. *Proceedings of the IEEE.* 1978;66(1):51-83.
57. Massoud Salehi P, Proakis J. *Digital Communications.* New York, NY: McGraw-Hill Education; 2007.
58. Blouin S, Barbeau M. An experimental baseline for underwater acoustic broadcasts In: Proceedings of the 2017 IEEE 86th Vehicular Technology Conference (VTC-Fall); 2017; Toronto, Canada.

59. Kassem J, Barbeau M, Ahmad A-M, Garcia-Alfaro J. The implementation of gnu radio blocks for decoding long-lasting frames in mobile underwater acoustic communications. In: Proceedings of the 8th Annual GNU Radio Conference; 2018; Henderson, NV. <https://pubs.gnuradio.org/index.php/grcon/article/view/50>. Accessed February 25, 2019.
60. Kassem J, Barbeau M, Ahmad A-M, Garcia-Alfaro J. GNU Radio blocks for long-lasting frames in mobile underwater acoustic communications. In: Proceedings of the French GNU Radio Days; 2018; Lyon, France. <https://gnuradio-fr-18.sciencesconf.org/211038/document>. Accessed February 25, 2019.

**How to cite this article:** Ahmad A-M, Barbeau M, Garcia-Alfaro J, Kassem J, Kranakis E. Tuning the demodulation frequency based on a normalized trajectory model for mobile underwater acoustic communications. *Trans Emerging Tel Tech*. 2019;e3712. <https://doi.org/10.1002/ett.3712>